Crystallization of Brownian particles in a pyramidal pit by a uniform external force

Crystallization of Brownian Particles in a Pyramidal Pit by a Uniform External Force

Youhei Kanatsu[1] and Masahide Sato[2]*

[1] *Graduate School of Natural Science and Technology, Kanazawa University, Kakuma, Kanazawa 920-1192, Japan*

[2] *Information Media Center, Kanazawa University, Kakuma, Kanazawa 920-1192, Japan*

We carry out Brownian dynamics simulations and study the crystallization of particles in an inverse pyramidal-shaped container induced by an external force. Owing to the side walls of the container, the face-centered cubic (fcc) structure is mainly formed. In the bulk, both disordered solidlike particles and hexagonal close-packed (hcp) structured particles are hardly formed. These two types of particle appear near the central axis of the container. Their numbers increase with increasing strength of the external force.

1. Introduction

Recently, the formation of large colloidal crystals has frequently been studied because these crystals can be used as photonic crystals. For example, close-packed colloidal crystals are used as photonic crystals with a perfect three-dimensional photonic band gap.[1)] One of the methods of creating the close-packed colloidal crystals is sedimentation. By simple sedimentation, however, random stacking occurs[2)] and many small polycrystals are formed, so that forming large single crystals of colloidal particles is difficult. Thus, to form large close-packed colloidal crystals, many groups add devices in a container.

Using a template, van Blaaderen et al.[3)] succeeded in creating large grains of a close-packed colloidal crystal with the face-centered cubic (fcc) structure. When colloidal particles are slowly sedimented on a patterned substrate, the crystallization of colloidal particles occurs, being reflected by the lattice pattern on the substrate, and large colloidal crystals are formed. This method is called colloidal epitaxy. Indeed, colloidal epitaxy is a potential method of forming large colloidal crystals. However, if the size of the colloidal particles is changed, it is necessary to prepare a lattice whose lattice constant is suitable for such particles.

*E-mail: sato@cs.s.kanazawa-u.ac.jp

To form a large grain of a colloidal crystal without defects, preparing a patterned substrate with an exact periodicity is also required.

Matsuo et al.[4] and Yin et al.[5] added contrivances to the container shape. In Ref. 4, the authors used an inverse pyramidal pit as a container and created a large colloidal crystal. Since an anisotropically wet etched pit was used in the experiment,[4] the angle of the apex of the inverse pyramidal pit was precisely set to be suitable. Thus, the {111} faces of the fcc structure were formed on the side walls of the pit and the growing interface became the {100} face of the fcc structure. On the {111} face of the fcc structure, two stacking methods of particles are possible, so that both the fcc structure and the hcp structure are easily formed. However, the stacking method of particles on the {100} face of the fcc structure is unique, so that defect formation is suppressed and large colloidal crystals with the fcc structure are formed regardless of the size of the colloidal particle. In Ref. 6, Mori et al. carried out a Monte Carlo simulation of hard spheres and reported the formation of colloidal crystals in a pyramidal pit, but their report is brief. We intend to study the crystallization of particles in a pyramidal pit in more detail.

In this study, keeping the formation of colloidal crystal in a pyramidal pit[4] in mind, we carry out Brownian dynamics simulations and study the crystallization of particles in a pyramidal pit induced by a uniform external force. In § 2, we introduce our model, in which a simple and standard algorithm is used. In § 3, we introduce the order parameters, which we use to determine the local structure. In § 4, we show our results. We investigate the process of crystallization and study the dependence of local structure on the strength of the external force. In § 5, we summarize our results.

2. Model

In our simulation, we use a simple algorithm[7] similarly to our previous studies.[8–12] We assume that particles move while receiving a uniform external force and resistance, which is proportional to their velocity. If the resistance is strong, the velocity of the ith particle is given by

$$\frac{d\boldsymbol{r}_i}{dt} = \frac{1}{\zeta}\left(F_{\mathrm{ext}}\mathbf{e}_{\mathrm{ext}} - \sum_{i\neq j} \boldsymbol{\nabla} U(r_{ij}) + \boldsymbol{F}_i^{\mathrm{B}} \right), \tag{1}$$

where $\boldsymbol{r}_i$ is the position of the ith particle and ζ is the frictional coefficient. The first term $F_{\mathrm{ext}}\mathbf{e}_{\mathrm{ext}}$ represents the uniform external force, where F_{ext} and $\boldsymbol{e}_{\mathrm{ext}}$ are the force strength and force direction, respectively. The second term represents the internal force from the other particles. We assume that the interaction potential between the ith and jth particles, $U(r_{ij})$,

is a short-range repulsive potential and a function of the distance between the two particles, $r_{ij} = |\boldsymbol{r}_i - \boldsymbol{r}_j|$. For simplicity, we use the Weeks-Chandler-Anderson (WCA) potential:[13)]

$$U(r_{ij}) = \begin{cases} 4\epsilon\left[\left(\dfrac{\sigma}{r_{ij}}\right)^{12} - \left(\dfrac{\sigma}{r_{ij}}\right)^{6} + \dfrac{1}{4}\right] & (r \le r_{\rm in}), \\ 0 & (r \ge r_{\rm in}), \end{cases} \tag{2}$$

where σ is the characteristic length representing the diameter of particles and $r_{\rm in} = 2^{1/6}\sigma$. In Eq. (1), the third term $\boldsymbol{F}_i^{\rm B}$ represents the isotropic random force, which satisfies the following relations:

$$\left\langle \boldsymbol{F}_i^{\rm B}(t) \right\rangle = \boldsymbol{0}, \tag{3}$$

$$\left\langle \boldsymbol{F}_i^{\rm B}(t) \cdot \boldsymbol{F}_j^{\rm B}(t') \right\rangle = 6\zeta k_{\rm B} T \delta_{ij} \delta(t - t'). \tag{4}$$

A simple normalized difference equation of Eq. (1) is given by[7)]

$$\tilde{\boldsymbol{r}}_i(\tilde{t} + \Delta\tilde{t}) = \tilde{\boldsymbol{r}}_i(\tilde{t}) + \left(\tilde{F}_{\rm ext}\mathbf{e}_{\rm ext} - \sum_{i \ne j} \boldsymbol{\nabla} U(r_{ij}) \right) \Delta\tilde{t} + \Delta\tilde{\boldsymbol{r}}_i^{\rm B}, \tag{5}$$

where the particle positions, time, and forces are scaled as $\tilde{\boldsymbol{r}}_i = \boldsymbol{r}_i/\sigma$ $\tilde{t} = t\epsilon/\zeta\sigma^2$, $\tilde{F}_{\rm ext} = F_{\rm ext}\sigma/\epsilon$, and $\tilde{\boldsymbol{F}}_{ik} = \boldsymbol{F}_{ik}\sigma/\epsilon$, respectively. The last term $\Delta\tilde{\boldsymbol{r}}_i^{\rm B}$, which presents the normalized isotropic displacement by the random force, satisfies

$$\left\langle \Delta\tilde{\boldsymbol{r}}_i^{\rm B}(t) \right\rangle = \boldsymbol{0}, \tag{6}$$

$$\left\langle \Delta\tilde{\boldsymbol{r}}_i^{\rm B}(t) \cdot \Delta\tilde{\boldsymbol{r}}_j^{\rm B}(t') \right\rangle = 6\tilde{R}^{\rm B}\Delta\tilde{t}\delta_{ij}\delta(t - t'), \tag{7}$$

where the scaled displacement by random force $\tilde{R}^{\rm B} = k_{\rm B}T/\epsilon$.

3. Order Parameters

In our simulation, since we use a short-range repulsive potential, both the fcc structure and the hexagonal close-packed (hcp) structure are expected to be formed in bulk. In order to distinguish the structure in solid, we introduce the order parameters $d_l(i, j)$, $Q_l(i)$, and $w_l(i)$. We use the order parameter $d_l(i, j)$[14,15)] to characterize the connection between the ith and jth particles. The definition of $d_l(i, j)$ is given by

$$d_l(i, j) = \sum_{m=-l}^{l} q_{l,m}(i) q_{l,m}^*(j), \tag{8}$$

where $q_{l,m}(i) = n_{\rm n}^{-1} \sum_{j=1}^{n_{\rm n}} Y_l^m(\theta_{ij}, \phi_{ij})$ and $q_{l,m}^*(j)$ is the complex conjugate of $q_{l,m}(j)$. $Y_l^m(\theta_{ij}, \phi_{ij})$ is the spherical harmonics and the angles θ_{ij} and ϕ_{ij} represent the polar and azimuthal angles, respectively. $n_{\rm n}$ is the number of neighboring particles. Since we use the WCA potential, the repulsion between the ith and jth particles acts when the distance between them is smaller

than $r_{\rm in}$. Thus, taking account of the random displacement, we regard the jth particle as a neighbor of the ith particle if $r_{ij} < 1.1r_{\rm in}$. When the ith and jth particles are neighbors and $d_6(i, j) > 0.7$, the connection between the two particles is solidlike. If the ith particle has four or more solidlike connections, the ith particle is considered a solidlike particle.

When the ith particle is a solidlike particle that has nine or more neighbors, we determine its local structure using $Q_l(i)$ and $w_l(i)$.[16–20] The parameters $Q_l(i)$ and $w_l(i)$ are defined as

$$Q_l(i) = \sqrt{\frac{4\pi}{(2l+1)}\sum_{m=-l}^{l}|q_{l,m}(i)|^2}, \tag{9}$$

$$w_l(i) = \left[\frac{4\pi}{(2l+1)}\right]^{3/2}\sum_{m_1+m_2+m_3=0}\begin{pmatrix} l & l & l \\ m_1 & m_2 & m_3 \end{pmatrix}\frac{q_{l,m_1}(i)q_{l,m_2}(i)q_{l,m_3}(i)}{Q_l(i)^3}. \tag{10}$$

The integers m_1, m_2, and m_3 change from $-l$ to l satisfying $m_1 + m_2 + m_3 = 0$. The term in parentheses in Eq. (10) is the Wigner 3-j symbol. In Ref. 11, we carried out a similar simulation, in which we used a cuboidal container. We investigated the distribution of the parameters Q_4 and w_4 in detail. We determined the parameter regions in which the solid structure is regarded as the hcp structure or the fcc structure, and succeeded in distinguishing the fcc structure from the hcp structure. Thus, in this study, we use the same parameter values: the local structure is regarded as the fcc structure if $-0.18 < w_4(i) < -0.01$ and $0.175 < Q_4(i) < 0.2$ and as the hcp structure if $0.02 < w_4(i) < 0.15$ and $0.06 < Q_4(i) < 0.15$ similarly to our previous studies.[10–12]

4. Results of Simulations

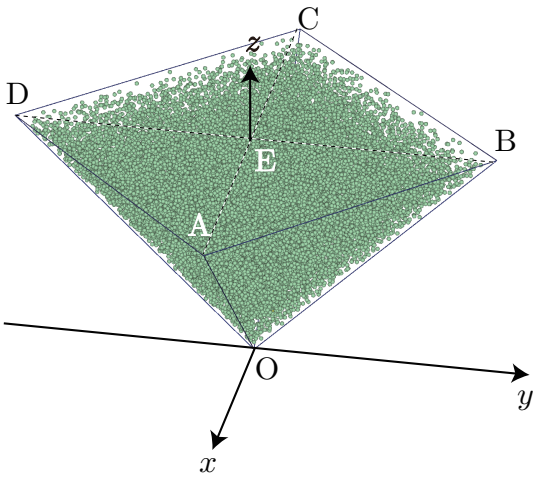

Fig. 1. (color online) A typical shape of a container and the particle positions in a very early stage ($\tilde{t} = 4.0$).

In Fig. 1, we show a typical container shape and positions of particles in a very early stage. We use an inverse pyramidal container, which is formed by four triangular walls, OAB, OBC, OCD, ODA, and a square wall ABCD. The particles act as hard spherical particles with the radius $\sigma/2$ for the walls, and elastic collisions occur between the walls and the particles. AC and BD are parallel to the x- and y-axes, respectively. The z-axis is on OE, where the point E is the center of the square wall ABCD. The normal directions of the side walls OAB, OBC, OCD and ODA, are $(-1,-1,1)$, $(1,-1,1)$, $(1,1,1)$, and $(-1,1,1)$, respectively. When the height of the pyramidal container is given by $\overline{\mathrm{OE}} = L$, the length of all the edges is given by $\sqrt{2}L$. By using the number of particles N and the volume fraction ϕ_0, the length L is expressed as $(\pi N/\sqrt{2}\phi_0)^{1/3}\sigma$. In our simulation, we set N, ϕ_0, and σ to $N = 23328$, $\phi_0 = 0.1$, and $\sigma = 1.0.$, respectively. Thus, the length L is given by $L = 56.8$. Initially, we put particles in the pyramidal container at random and move the particles without an external force. Then, we set the time to 0. We add an external force in the negative z direction and move the particles.

In our simulations, the strengths of the random force and external force are $\tilde{R}_{\mathrm{B}} = 0.1$ and $\tilde{F}_{\mathrm{ext}} = -0.2$, respectively. In Fig. 2, we show the cross sections cut on the plane OBD, which are seen from the positive x-direction. In the figures, we regard the solid particles attached to the walls as disordered solidlike particles because we cannot determine whether they have the hcp structure or the fcc structure. In an early stage [Fig. 2(a)], almost all the particles are liquidlike, Only near the apex O, solidification occurs and a few fcc-structured particles are formed. With increasing time [Fig. 2(b)], solidification proceeds and the number of the fcc-structured particles increases. Solidification around the edges OB and OD seems to be slightly faster than that on the side walls. In the late stage [Fig. 2(c)], sedimentation ends. Most of the particles are the fcc-structured particles and liquidlike particles. The fcc-structured particles are present on the lower side and the liquidlike particles form layers on the fcc-structured particles. Between the liquidlike particles and the fcc-structured particles, a thin layer of the disordered solidlike particles is formed. The number of disordered particles near the center of the interface is larger than that in other places. A few particles with the hcp structure are present in the layer of the disordered particles. Figure 3 shows a snapshot in the late stage with $F_{\mathrm{ext}} = -0.4$. In comparsion with that showed in Fig. 2, the width of the disordered particles is smaller and the number of disordered solids in the fcc-structured bulk is larger, which are caused by the strong external force. The hcp-structured particles also increase in number, and they form sheets parallel to the wide walls.

In Figs. 2 and 3, we observed how solidification proceeds in the vertical direction. Next,

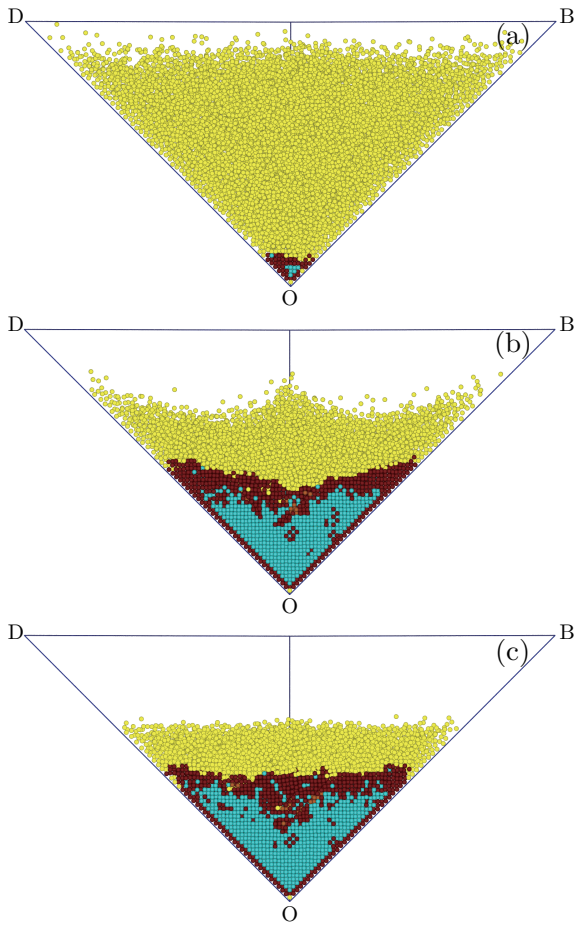

Fig. 2. (color online) Snapshots of cross sections cut on the plane OBD in (a) an early stage ($\tilde{t} = 56$), (b) a middle stage ($\tilde{t} = 200$), and (c) a late stage ($\tilde{t} = 400$). The particles are classified into four types, liquidlike particles, fcc-structured particles, hcp-structured particles, and disordered solidlike particles. They are colored yellow (the lightest), blue (the second lightest), orange (the third lightest), and red (dark), respectively.

we show how solidification proceeds in the horizontal direction. Figure 4 shows the cross sections whose z-coordinate is 19.5. When $\tilde{t} = 112$ [Fig. 4(a)], many liquidlike particles are present at the center of the plane, and some disordered solidlike particles appear near four ridge lines. When $\tilde{t} = 128$ [Fig. 4(b)], solidification proceeds and the region with the disordered solidlike particles spreads. The liquidlike particles are left near the center of the container. Near the wall, the crystallization of solid particles starts and a few fcc particles appear. When $\tilde{t} = 164$ [Fig. 4(c)], the liquidlike particles are hardly left. The area of the region with the fcc structure increases and a few hcp-structured particles are observed. In our previous studies,[8–12] in which the container was cuboid or rhomboid, the two-dimensional ordering along the walls of the container first occurred. Then, the crystallization in bulk proceeded, being affected by the two-dimensional order on the walls. In the present case, the

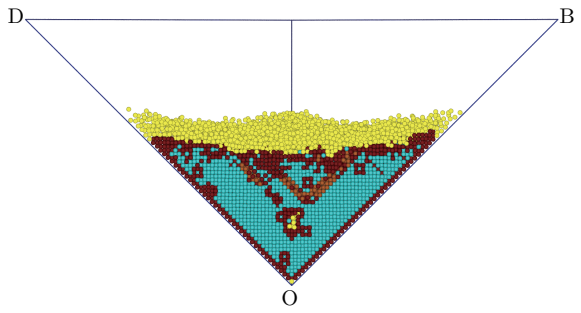

Fig. 3. (color online) Snapshots of cross sections cut on the plane OBD in a late stage ($\tilde{t} = 200$) with $F_{\rm ext} = -0.4$. The meanings of the colors of particles are same as those in Fig. 2.

container shape is different from those in the previous studies, but the crystallization process is the same. When we see the same z-level, the crystallization proceeds from the side walls to the center of the container. Since the effect of the walls on the crystallization is strong, the disordered particles hardly remain near the walls. However, in the center region in the plane, the effect of the crystallization on the walls decreases. Thus, disordered particles tend to remain there.

Table I. Dependences of the numbers of four types of particle on $\tilde{F}_{\rm ext}$. We count the numbers of each type of particle in the steady state. $N_{\rm hcp}$, $N_{\rm fcc}$, $N_{\rm solid}$, and $N_{\rm liquid}$ represent the hcp-structured particle number, the fcc-structured particle number, the disordered solidlike number, and the liquidlike particle number, respectively. The data are averaged over 10 samples.

$\tilde{F}_{\rm ext}$	$N_{\rm hcp}$	$N_{\rm fcc}$	$N_{\rm solid}$	$N_{\rm liquid}$
-0.2	289.80 ± 33.65	5031.60 ± 109.52	5839.80 ± 104.18	10049.40 ± 36.22
-0.4	848.60 ± 76.56	8922.30 ± 115.09	5403.10 ± 65.13	5482.10 ± 10.92
-0.8	1539.10 ± 112.49	10871.30 ± 160.23	4767.00 ± 52.70	3045.30 ± 13.82
-1.0	1655.40 ± 40.41	11889.30 ± 81.33	4444.30 ± 50.47	2279.10 ± 13.18

In our simulation, since the angle of the apex of the pyramidal container is suitable, a triangular lattice, which acts as the {111} face of the fcc structure, is formed on the walls. Being affected by the walls, the fcc structure grows in bulk. The growing interface is roughly parallel to the xy plane, so that the interface is one of the {100} faces of the fcc structure. Since the stacking method of particles on the {100} plane of the fcc structure is unique, the defect formation is suppressed. From the snapshots showed in Figs. 2 and 4, we already confirmed that the fcc structure is mainly formed in bulk, which agrees with the experiments.[4)] Here, to study the dependence of structures in bulk on the force strength, we estimate the numbers of

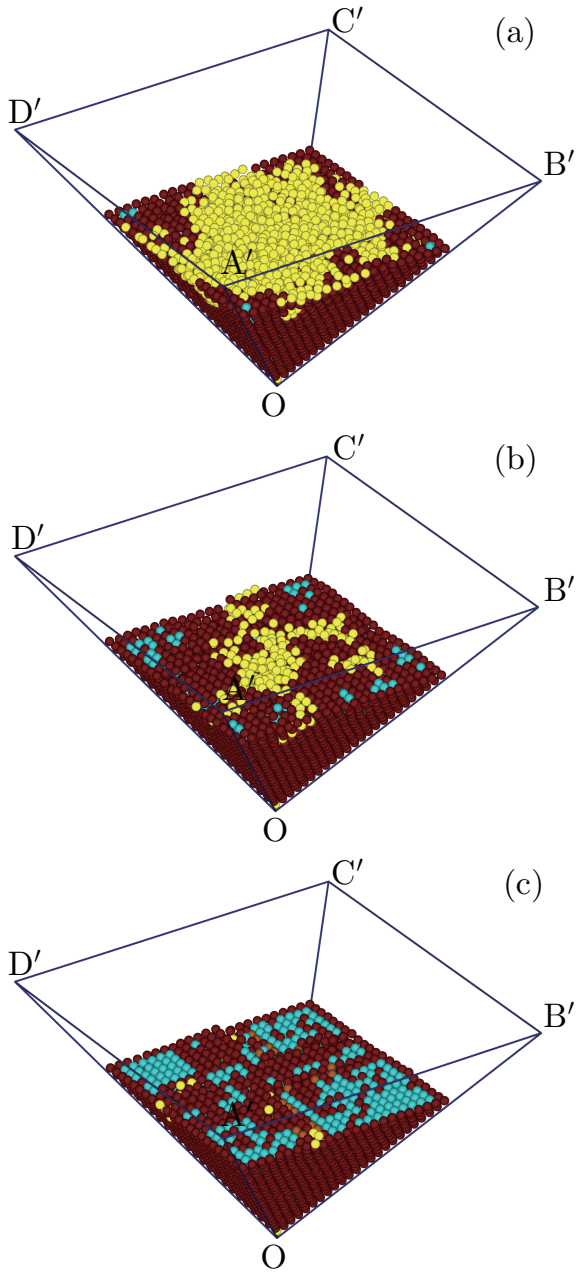

Fig. 4. (color online) Snapshots of cross sections cut at $z = 19.5$. Times $\tilde{t}$ are (a) 112, (b) 128, and (c) 164. A′=OA/2, OB′=OB/2, OC′=OC/2, OD′=OD/2. The meanings of the colors of the particles are the same as those in Fig. 2.

each type of particle more precisely. We show the dependences of the numbers of four types of particle on $\tilde{F}_{\rm ext}$ in Table I, where we omit the particles attached to the walls. $N_{\rm hcp}$, $N_{\rm fcc}$, $N_{\rm solid}$, and $N_{\rm liquid}$ represent the numbers of the hcp-structured particles, the fcc-structured particles, solidlike particles, and liquidlike particles, respectively. On the upper side of the container, the particles are not pressed strongly by other particles. Thus, both the liquidlike particles and

the disordered solidlike particles are left on the top of the ordered particles. When $F_{\rm ext} = 0.2$, which is the weakest external force in our simulation, both $N_{\rm solid}$ and $N_{\rm liquid}$ are large: $N_{\rm solid}$ is about as large as $N_{\rm fcc}$, and $N_{\rm liquid}$ is about twice as large as $N_{\rm solid}$. When the particles are pressed by a strong external force, both $N_{\rm solid}$ and $N_{\rm liquid}$ decrease. In particular, the decrease is larger in $N_{\rm liquid}$ than in $N_{\rm solid}$. On the other hand, both $N_{\rm hcp}$ and $N_{\rm fcc}$ increase with increasing $\tilde{F}_{\rm ext}$. $N_{\rm hcp}$ is much smaller than $N_{\rm fcc}$ regardless of the strength of the external force, but the ratio of $N_{\rm hcp}$ to $N_{\rm fcc}$ increases with increasing $\tilde{F}_{\rm ext}$.

Hereafter, we investigate where each type of particle appears in the steady state. First, we cut the solid phase at several heights and see the crystallization of particles in the cross sections. Figure 5 shows the cross sections in a late stage ($\tilde{t} = 800$). Near the apex of the pyramidal container [Fig. 5(a)], the bulk consists of the fcc structure. The other types of particle are not seen. With increasing z-coordinate [Fig. 5(b)], the disordered solidlike particles and the liquidlike particles appear. They form a small cluster near the center of the container. When the z-coordinate of the cross section approaches that of the liquid-solid interface, the number of disordered solidlike particles increases. In Fig. 5(c), a few of the hcp-structured particles and liquidlike particles are also seen.

In Fig. 6, we show the z-dependences of the densities of all types of particle in the final stage. We cut the container parallel to the xy plane into thin circular truncated cones whose width is $\Delta L = \overline{\rm OE}/25$, and estimate the densities of the four types of particle in the circular truncated cones. Note that the sum of the densities at each height is not equal to unity because we omit the particles attached to the container walls. Figure 6(a) shows the profiles of the densities with $\tilde{F}_{\rm ext} = 0.2$. Near the apex O, except for the particles attached to the walls, almost all the particles are the fcc-structured particles. With increasing height, the density of the fcc-structured particles increases and its maximum appears at about $z = 12$. Then, the density decreases and the fcc-structured particles vanish at about $z = 30$. In the low region, the number of disordered solidlike particles increases gradually with increasing z-coordinate. When the number of fcc-structured particles starts to decrease, the increase in the number of disordered solidlike particles is accelerated and the maximum density appears at $z \simeq 28$. The disordered solidlike particles vanish at $z = 30$. The hcp-structured particles appear in the region where $10 < z < 30$, which is much narrower than the region where the fcc-structured particles are present, and the density of the particles is much lower than that of the fcc-structured particles. The liquidlike particles are present in a narrow region where $24 < z < 40$. The maximum density of the liquidlike particles is as high as that of the disordered solidlike particles.

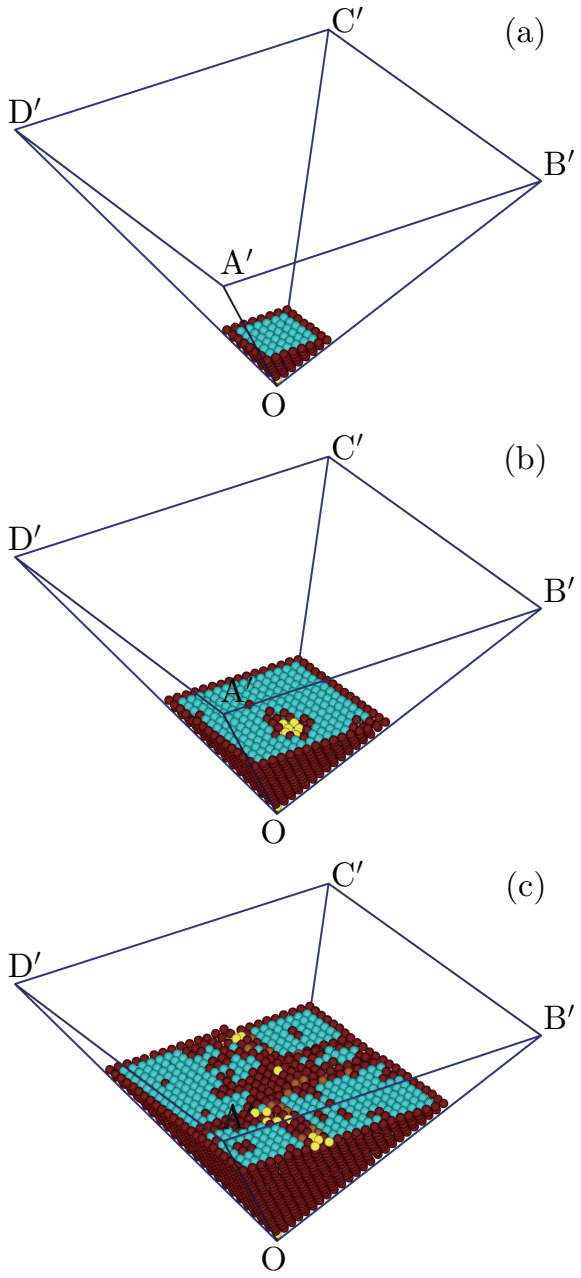

Fig. 5. (color online) Snapshots of cross sections parallel to the *xy* plane in a late stage ($\tilde{t}$ = 800). The *z* coordinates of the cross sections are (a) 6.8, (b) 12.8, and (c) 19.5. OA′=OA/2, OB′=OB/2, OC′=OC/2, OD′=OD/2. The meaning of the colors of the particles are the same as those in Fig. 2.

When $\tilde{F}_{\mathrm{ext}}$ = 0.4 [Fig. 6(b)], the maximum densities of the disordered solidlike particles and liquidlike particles become lower, and the width where the liquidlike particles are present is smaller than those in Fig. 6(a). In the low-*z*-coordinate region, the densities of the disordered solidlike particles and hcp-structured particles in bulk are higher than those shown in Fig. 6(a). However, to the stacking method on the {100} face is unique, defect formation is

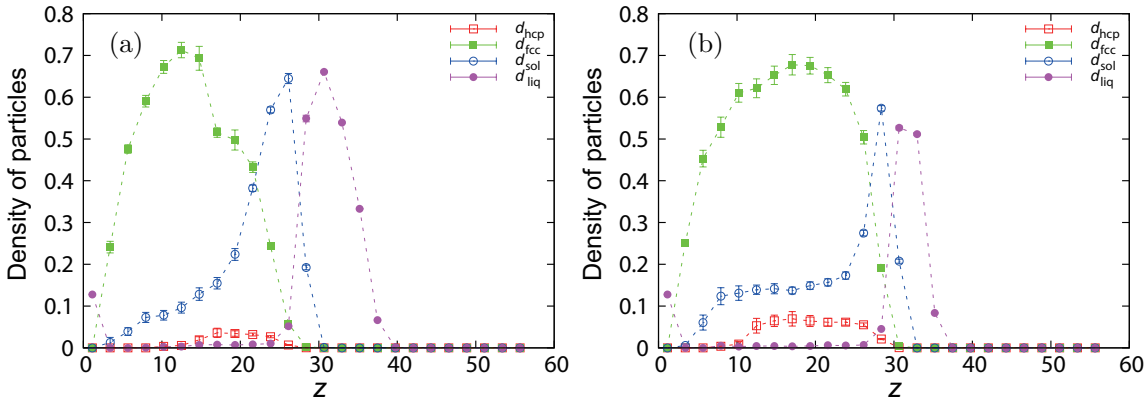

Fig. 6. (color online) Dependence of the densities of particles on the container height in the late stage. $d_{\rm hcp}$, $d_{\rm fcc}$, $d_{\rm sol}$, and $d_{\rm liq}$ represent the densities of the hcp-structured particles, the fcc-structured particles, disordered solidlike particles, and liquidlike particles, respectively. The strengths of the external force are (a) $\tilde{F}_{\rm ext} = 0.2$, and (b) $\tilde{F}_{\rm ext} = 0.4$. The data are averaged over 10 individual runs.

necessary to form hcp-structured particles. The disordered particles left in bulk act as defects and induced the formation of the hcp structure. The hcp structure appears like sheets parallel to the {111} face, on which the stacking faults are formed easily. Thus, regardless of the force strength, the disordered solidlike particles first appear in the low-z-coordinate region before the hcp-structured particles are produced.

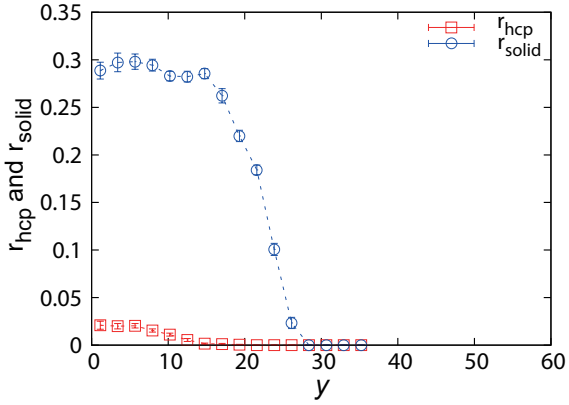

Fig. 7. (color online) Distributions of the hcp-structured particles and disordered solidlike particles in the y-direction. The ratios $r_{\rm hcp}$ and $r_{\rm solid}$ represent the ratios of the hcp-structured particles and disordered solidlike particles in the late stage ($\tilde{t} = 800$). The data are averaged over 10 individual runs.

Finally, we show how the hcp-structured particles and disordered solidlike particles are distributed in the y-direction. We cut the container parallel to the xz plane into small truncated triangular cones. We count the number of particles in the regions, $\Delta N(y)$, and derive the ratios

$r_{\rm hcp}$ and $r_{\rm solid}$, which are the ratios of the numbers of hcp-structured particles and disordered solidlike particles to $\Delta N(y)$. Both $r_{\rm hcp}$ and $r_{\rm solid}$ are large near the center of the container. From Figs. 6 and 7, we consider that the formation of the disordered solidlike particles is needed to form the hcp structure. When the disordered solidlike particles are formed in the fcc structure, the particles attached to the disordered solidlike particles can assume the hcp structure. The formation of the disordered solidlike structure is the trigger for the formation of the hcp-structured particles.

5. Summary

In this work, we studied the crystallization of Brownian particles by sedimentation in a pyramidal pit. Using the order parameters, we determined the local structure. When we choose a suitalbe angle of the apex, the side walls act as the {111} faces of the fcc structure and the growing interface becomes the {100} face of the fcc structure. Since the stacking method of particles on the {100} face of the fcc structure is unique, defect formation is suppressed and the fcc structure is formed. During solidification, the crystallization of particles on the side walls of container occurs first. Then, the solidification proceeds inwards. Thus, if disordered particles are left, their density is high at the center of the container. The disordered particles induce the formation of the layers of hcp-structured particles. The layers are parallel to the side walls and consist of the {111} planes, on which the stacking faults are easily produced.

In Ref. 4, polystyrene particles whose diameter $\sigma = 1.038$ μm were used as colloidal particles, and the gravitational sedimentation in a pyramidal pit was carried out. The densities of the polystyrene, $\rho_{\rm P}$, and water, $\rho_{\rm W}$, are given by $\rho_{\rm p}$ =1.05 g/cm^2 and $\rho_{\rm w}$ =1.00 g/cm^2, respectively. Thus, the external force is given by $F_{\rm ext} = 4\pi(\rho_{\rm p} - \rho_{\rm w})(\sigma/2)^3 g = 2.89 \times 10^{-16}$ N, where we use $g = 9.8$ m/s^2 as the gravitational acceleration. When the temperature $T = 300$ K and we use the particle radius as a characteristic length, the Peclet number is estimated as $F_{\rm ext}(\sigma/2)/k_{\rm B}T = 3.6\times10^{-2}$. In our simulation, the Peclet number is given by $F_{\rm ext}(\sigma/2)/k_{\rm B}T = \tilde{F}_{\rm ext}/2\tilde{R}_{\rm B} = 1$ - 10. Since the sedimentation velocity in our simulation is much faster than that in the experiment,[4] defects are formed more easily than in the experiment.[4] However, the crystallization process in our simulation is qualitatively similar to that in the experiment.

In our simulations, the liquidlike particles are left on the top of the solid phase with a weak external force. To increase the number of solidlike particles, we need a strong force. With increasing the strength of the external force, however, the sedimentation velocity increases and crystallization proceeds before the particles settle in suitable positions, so that the number of disordered particles increases in bulk. If we gradually increase the external force, many fcc-

structured particles may be formed without formation of disordered solidlike particles in the lower region. Thus, we intend to study the change in the external force in detail.

Acknowledgments

M. S. thanks Y. Suzuki and H. Katsuno for reading this paper carefully and giving fruitful comments. This work was supported by KAKENHI Grant Numbers 26103515, 26390054 from the MEXT, Japan. M. S. benefited from the Joint Research Program of the Institute of Low Temperature Science, Hokkaido University.

References

1) A. Blanco, E. Chomski, S. Grabtchak, M. Ibisate, S. John, S. W. Leonard, C. Lopez, F. Meseguer, H. Miguez, J. P. Mondia, G. A. Ozin, O. Toader, and H. M. Van Diel, Nature **405**, 437 (2000).
2) P. N. Pusey, W. V. Megen, P. Bartlett, B. J. Ackerson, J. G. Rarity, and S. M. Underwood, Phys. Rev. Lett. **63**, 2753 (1989).
3) A. von Blaaderen, R. Ruel, and P. Wiltzius, Nature (London) **385**, 321 (1997).
4) S. Matsuo, T. Fujine, K. Fukuda, S. Juodkazis, and H. Misawa, Appl. Phys. Lett. **82**, 4285 (2003).
5) Y. Yin, Z.-Y. Li, and Y. Xia, Langmuir **19**, 622 (2003).
6) A. Mori, Y. Suzuki, and S. Matsuo, Prog. Theor. Phys. Suppl. **178**, 33 (2009).
7) D. L. Ermak, J. Chem. Phys. **62**, 4189 (1975).
8) M. Sato, H. Katsuno, and Y. Suzuki, Phys. Rev. E **87**, 032403 (2013).
9) M. Sato, H. Katsuno, and Y. Suzuki, J. Phys. Soc. Jpn. **82**, 084804 (2013).
10) M. Sato, Y. Suzuki, and H. Katsuno, J. Cryst. Growth **401**, 87 (2014).
11) M. Fujine, M. Sato, H. Katsuno, and Y. Suzuki, Phys. Rev. E **89**, 042401 (2014).
12) M. Fujine, M. Sato, T. Toyooka, H. Katsuno, Y. Suzuki, and T. Sawada, Phys. Rev. E **90**, 032404 (2014).
13) J. D. Weeks, D. Chandler, and H. C. Anderson, J. Chem. Phys. **54**, 5237 (1971).
14) P. R. ten Wolde, M. J. Ruiz-Montero, and D. Frenkel, Phys. Rev. Lett. **75**, 2714 (1995).
15) M. Marechal, M. Hermes, and M. Dijkstra, J. Chem. Phys. **135**, 034510 (2011).
16) P. J. Steinhardt, D. R. Nelson, and M. Ronchetti, Phys. Rev. B **28**, 784 (1983).
17) M. D. Rintoul and S. Torquato, J. Chem. Phys. **105**, 9258 (1996).
18) W. Lechner and C. Dellago, J. Chem. Phys. **129**, 114707 (2008).
19) A. Panaitescu, K. A. Reddy, and A. Kudrolli, Phys. Rev. Lett. **108**, 108001 (2012).
20) C. Desgranges and J. Delhommelle, Phys. Rev. B **77**, 054201 (2008).